Active approach for holographic non-destructive testing of satellite fuel tanks

Torsten Merz[a], Frank Elandaloussi[b], Dietrich Paulus[a], Wolfgang Osten[b]

[a] Universität Erlangen-Nürnberg, Lehrstuhl für Mustererkennung
Martensstr. 3, D-91058 Erlangen, Germany
[b] Bremer Institut für angewandte Strahltechnik (BIAS)
Klagenfurter Str. 2, D-28359 Bremen, Germany

ABSTRACT

In computer vision several views exist how to solve vision problems. The first general methodology was introduced by Marr; he proposed a data-driven and straightforward analysis strategy. Nowadays the concept of *active vision* introduced by Aloimonos et al. becomes more and more important. In contrast to Marr's philosophy, active vision implies a feedback loop which consists of sensors and active components. In this paper we present a system for the identification of material faults under the surface of a test object. For that purpose the specimen is elastically deformed, then the deformation is made visible using holographic interferometry, and finally flaw parameters are estimated using a model-based approach to analyze interferograms. This is an underconstrained computer vision problem which is regularized using a priori knowledge and an active modification of the experimental setup. More mathematically, this vision task can be seen in the context of inverse problem theory. In this contribution we describe the system and point out how it is related to the methodologies named above. To illustrate the functionality of the system, results are shown from non-destructive testing of satellite fuel tanks.

Keywords: holographic non-destructive testing, interferogram analysis, parameter estimation, inverse problems, active vision, image processing

1. INTRODUCTION

The problems in optical metrology are very similar to those of computer vision. Both disciplines deal with image–like input and use image processing techniques to derive a symbolic description of the image content or to reconstruct various quantities from the acquired intensity distribution. Examples can be found in experimental shape and stress analysis (ESA) where geometrical and mechanical quantities such as coordinates and displacements have to be derived from periodically modulated intensity distributions or in holographic non-destructive testing (HNDT) where the observed fringe patterns must be analyzed with respect to the detection of material faults. In this contribution we will describe an active approach for automatic HNDT of satellite fuel tanks and show its relation to inverse problem theory. The term "active" means that the load of the specimen is changed in a flexible way depending on the deformation behaviour and the kind of possible material faults.

The well known paradigm of Marr

> "Computer vision is the development of procedures for the solution of the inverse task of the image formation process"[1]

describes nothing else than the task to conclude from the effect to its cause. In holographic interferometry, the intensity $I(i,j)$ at pixel location (i,j) is used to determine the cause, in that case the displacement $d(x,y,z)$ of the related object point (x,y,z). In other words, an inverse problem has to be solved. But what is an inverse problem?

From the point of view of a mathematician the concept of an inverse problem has a certain degree of ambiguity which is well illustrated by a frequently quoted statement of J.B. Keller[2]:

Further author information:
E-mail: [a]merz@informatik.uni-erlangen.de, [b]fe@elanda.bias.uni-bremen.de
WWW: [a]http://www5.informatik.uni-erlangen.de, [b]http://www.bias.uni-bremen.de

"We call two problems inverses of one another if the formulation of each involves all or part of the solution of the other. Often for historical reasons, one of the two problems has been studied extensively for some time, while the other has never been studied and is not so well understood. In such cases, the former is called direct problem, while the latter is the inverse problem."

Both problems are related by a kind of duality in the sense that one problem can be derived from the other by exchanging the role of the data and that of the unknown: the data of one problem are the unknowns of the other and vice versa. As a consequence of this duality it may seem arbitrary to decide what is the direct and what is the inverse problem. For physicists and engineers, however, the situation is quite different because the two problems are not on the same level:[3] one of them, and precisely the one called the direct problem, is considered to be more fundamental than the other and, for this reason is also better investigated. Consequently the historical reasons mentioned by KELLER are basically physical reasons. Processes with a well-defined causality such as the process of image formation are called direct problems. Direct problems need information about all quantities which influence the unknown effect. Moreover, the internal structure of causality, all initial and boundary conditions and all geometrical details have to be formulated mathematically.[4] Initial and boundary value problems which are usually expressed by ordinary and partial differential equations, are typical examples.

One example is KIRCHHOFF'S formulation of the diffraction problem: the direct problem consists in the computation of the scattered waves from the knowledge of the sources and obstacles. Such direct problems have some excellent properties which make them so attractive for physicists: If reality and mathematical description fit sufficiently well, the direct problem is expected to be uniquely solvable. Further on it is in general stable. That means, small changes of the initial or boundary conditions cause also small effects only (in contrast to chaotic processes). Unfortunately, numerous problems in physics and engineering deal with unknown but non-observable values. If the causal connections are investigated backwards we come to the concept of inverse problems. Based on indirect measurements, i.e. the observation of effects caused by the quantity we are looking for, one can try to identify the missing parameters. Such identification problems are well known in optical metrology. For instance the recognition and interpretation of subsurface flaws using HNDT[5,6] and the reconstruction of phase distributions[7] from the observed intensity values are quite common. However, inverse problems have usually some undesirable properties: they are in general ill–posed, ambiguous, and unstable. The concept of well-posedness was introduced by HADAMARD[8] into the mathematical literature. He defined a CAUCHY problem of partial differential equations as well-posed, if for all CAUCHY data there is a uniquely determined solution depending continuously on the data; otherwise the problem is ill–posed.

In mathematical notation, an operator equation

$$F(x) = y$$

is defined as well-posed with a linear operator $F \in \pounds(X, Y)$ in Banach spaces X and Y if the following three Hadamard conditions are satisfied:[8]

1. $F(x) = y$ has a solution $x \in X$ for all $y \in Y$ (existence),
2. This solution x is determined uniquely (uniqueness),
3. The solution x depends continuously on the data y, i.e. the convergence $||y_n - y|| \to 0$ of a sequence $y_n = F(x_n)$ implies the convergence $||x_n - x|| \to 0$ of corresponding solutions (stability).

If at least one of the above conditions is violated, then the operator equation is called ill-posed. Simply spoken ill-posedness means that we have not enough information to solve the problem uniquely. For the solution of inverse/ill-posed problems it is important to apply a maximum amount of a-priori knowledge or predictions about the physical quantities to be determined and we always have to answer the question if the measured data contain enough information to determine the unknown quantity uniquely. In case where the data y result from the integration of unknown components, thus this results in smoothing. The direct problem is also a problem directed towards a loss of information: its solution defines a transition from a physical quantity with a certain information content to another quantity with a smaller information content. This implies that the solution is much smoother than the corresponding object. For example, the scattered wave due to an obstacle is smooth even if the obstacle is rough.[3] Consequently, the information about any single component is lost and very different causes may give almost the same effect after integration. A well–known example for specialists in HNDT is the ambiguous relation between an observed fringe pattern (the effect) on the surface and its corresponding cause (one or several subsurface flaws) under the surface. The response of the flaw on the applied load is smoothed since only the displacement on the surface gives rise to the observed fringe pattern. These fringe patterns are very noisy and their topology is strongly limited.[5] Therefore the conclusion from the observed pattern to the cause behind is ambiguous in case of simple and straightforward inspection procedures. Later we will come back to this example. In order to overcome the disadvantages of ill-posedness in the process of finding an approximate solution to an inverse problem, different techniques of regularization are used. Regularizing an inverse problem means that instead of the ill-posed original problem a well-posed neighboring problem has to be formulated. The key decision of regularization is to find out an admissible compromise between stability and approximation.[4] As a consequence one cannot expect that the properties of the solution of the auxiliary problem coincide with the properties of the original problem. But convergence between the regularized and the original solution should be guaranteed if the stochastic character of the experimental data is decreasing. In case of noisy data the identification of unknown quantities can be considered as an estimation problem. Depending on the linearity or non-linearity of the operator F, we than have linear and non-linear regression models, respectively. Consequently, least-square methods play an important role in the solution of inverse problems:

$$||F(x) - y_\epsilon|| \rightarrow min \quad \text{with} \quad y_\epsilon = y + \epsilon$$

Several regularization techniques are based on the Thikonov regularization theory.[9,10]

Active vision/metrology is a direct way to handle the difficult regularization problem.[11] This is ensured by formulating an adequately stable auxiliary problem and by adding systematically more knowledge about the object under test and the method of its investigation into the evaluation process. A practical way to do that is the implementation of a feedback loop including the image formation process to create an expectation controlled data input. We now turn our attention to a special class of images that is relevant for optical metrology: fringe patterns. Some evaluation methods are discussed which shall illustrate the difference between direct and inverse problems as well the different approaches to handle inverse problems.

In the following sections, we first look at the inverse problem of flaw parameter estimation from fringe patterns in general and then propose our approach for solving the problem. We use data flow diagrams for the illustration of functional dependences. Data flow diagrams were first used in structured analysis.[12] They consists of processes or functions (boxes with round corners), data flows (arrows), data sets (two lines), and data sources or sinks (boxes with sharp corners). The execution flow is not explicitly defined, a process is executed if all required input data are available. A process can be refined by a further data flow diagram.

2. DIRECT AND INVERSE PROBLEMS

In general, recognition of material faults from fringe patterns can be formulated as an inverse parameter identification problem. A parametric geometric model is used to describe possible flaws. We assume multiple flaws being mutually independent and separable in space. The direct problem, i.e. the calculation of observable intensities given a parameter vector, is well understood and well-posed, whereas the inverse problem is difficult and ill-posed. For a better understanding of the inverse problem we decompose the problem into several functions. The functional dependences are illustrated in Fig. 1. In the following sections each function F and its inverse F^{-1} are explained.

2.1. Functions F_{ad} and F_{ad}^{-1}

The key function of the system is F_{ad}. It describes the calculation of displacement vectors $\boldsymbol{d}$ given the parameter vector $\boldsymbol{a}$. For HNDT of satellite fuel tanks a typical flaw is modeled by an ellipsoid with 6 parameters: center of ellipsoid, main axis, ancillary axis, and alignment of main axis. A geometric model of the tank is created by integrating the ellipsoid into a given exact model of the flawless tank. The deformation of the tank under a given load is calculated by a finite-element method.

For our purpose we are interested in the inverse function F_{ad}^{-1}, i.e. estimating the parameters $\boldsymbol{a}$ given a set of displacement vectors $\boldsymbol{d}$. This ill-posed problem is not very well understood in general, although there exist some investigations for some special cases.[6] More specific investigations for the ellipsoidal model, especially concerning functional dependencies, uniqueness, and stability of the solution, have to be done in future works. Up to now we cannot solve this problem in a direct way. Instead, we propose an iterative solution in Sections 2.4 and 3.

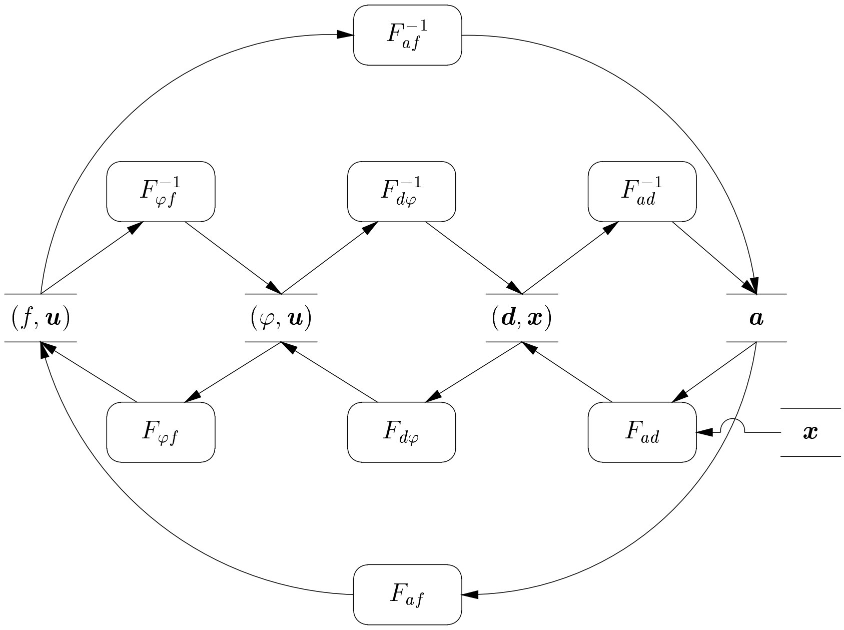

Figure 1. Data flow diagram of direct problems F and inverse problems F^{-1}: $\boldsymbol{x}$ object points, $\boldsymbol{a}$ flaw parameters, $\boldsymbol{d}$ displacements, $\boldsymbol{u}$ image points, φ phases, f intensities

2.2. Functions $F_{d\varphi}$ and $F_{d\varphi}^{-1}$

Function $F_{d\varphi}$ describes the calculation of phase differences φ of the interfering wave fields from displacement vectors. In the following we apply the concept of homologous points,[13] i.e. only corresponding object point pairs contribute to the formation of holographic interference pattern. Each object point $\boldsymbol{x}$ is projected to a corresponding image point $\boldsymbol{u}$. Contributions from other object points produce speckle noise. The phase difference is calculated by the inner product of the displacement of an object point and the corresponding sensitivity vector $\boldsymbol{s}_x$:[13]

$$F_{d\varphi}(\boldsymbol{d}, \boldsymbol{x}) = (\varphi, \boldsymbol{u}) = (< \boldsymbol{d}, \boldsymbol{s}_x >, F_{xu}(\boldsymbol{x})) \quad \boldsymbol{s}_x = F_{xs}(\boldsymbol{x})$$

Function F_{xs} is used for calculation of sensitivity vectors. It can be derived for spherical wavefronts from the position of the beam expander and the position of the optical center of the camera relative to the object and for plane waves from the wave propagation vectors. Function F_{xu} is described below.

For the calculation of displacement vectors from phase distributions we have to solve the inverse problem $F_{d\varphi}^{-1}$. There are at least three phase differences from different viewing or illumination directions necessary for a unique solution:[13]

$$F_{d\varphi}^{-1}(\varphi_1, \varphi_2, \varphi_3, \boldsymbol{u}) = (\boldsymbol{d}, \boldsymbol{x}) = \left(\begin{pmatrix} F_{xs_1}(\boldsymbol{x}_u)^t \\ F_{xs_2}(\boldsymbol{x}_u)^t \\ F_{xs_3}(\boldsymbol{x}_u)^t \end{pmatrix}^{-1} \begin{pmatrix} \varphi_1 \\ \varphi_2 \\ \varphi_3 \end{pmatrix}, \boldsymbol{x}_u \right) \quad \boldsymbol{x}_u = F_{xu}^{-1}(\boldsymbol{u})$$

The functions F_{xu} and F_{xu}^{-1} transform object points $\boldsymbol{x}$ to corresponding image points $\boldsymbol{u}$ and vice versa. These are classical problems from three-dimensional computer vision. If we assume a distortion-free pinhole camera model, the projection of object points given in homogeneous object coordinates $\tilde{\boldsymbol{x}}$ to image points given in homogeneous image coordinates $\tilde{\boldsymbol{u}}$ can be written using the homogeneous version of F_{xu} as:[14]

$$\boldsymbol{P} : \mathcal{P}^3 \to \mathcal{P}^2 \quad \tilde{\boldsymbol{x}} \in \mathcal{P}^3 \quad \tilde{\boldsymbol{u}} \in \mathcal{P}^2 \quad \tilde{F}_{xu}(\tilde{\boldsymbol{x}}) = \tilde{\boldsymbol{u}} = \boldsymbol{P}\,\tilde{\boldsymbol{x}}$$

In case of a plane object surface the projection can be simplified by choosing a two-dimensional coordinate system in the object plane, transforming the object points in homogeneous plane coordinates $\tilde{\boldsymbol{x}}_p$, and applying a collineation of projective space:[14]

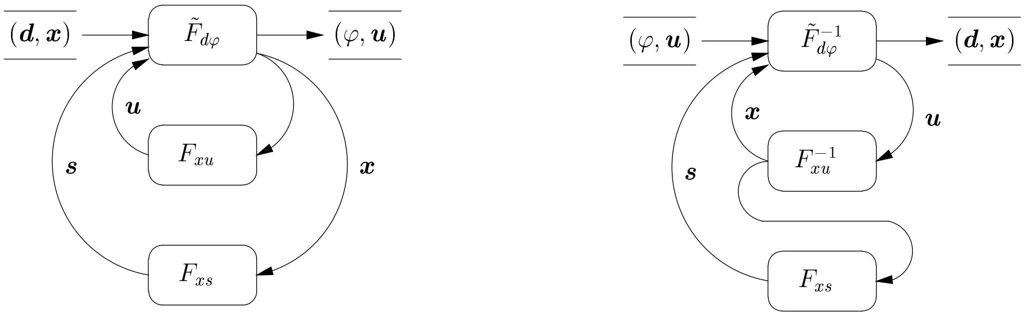

Figure 2. Data flow diagrams of phase difference calculation from displacement vectors and the inverse function

$$\boldsymbol{P}_p : \mathcal{P}^2 \rightarrow \mathcal{P}^2 \quad \tilde{\boldsymbol{x}}_p \in \mathcal{P}^2 \quad \tilde{\boldsymbol{u}} \in \mathcal{P}^2 \quad \tilde{F}_{xu}(\tilde{\boldsymbol{x}}_p) = \tilde{\boldsymbol{u}} = \boldsymbol{P}_p\, \tilde{\boldsymbol{x}}_p$$

In the latter case corresponding object points can be calculated easily from given image points by inverting the collineation matrix $\boldsymbol{P}_p$:

$$\tilde{F}^{-1}_{xu}(\tilde{\boldsymbol{u}}) = \tilde{\boldsymbol{x}}_{\boldsymbol{p}} = \boldsymbol{P}_p^{-1}\tilde{u}$$

In the general case the inversion of F_{xu} is not unique. Nevertheless a unique solution exists, if only visible object points are considered. Raytracing methods are used to find corresponding, visible object points.

In Fig. 2 the functions for calculating phase differences from displacement vectors and vice versa are summarized.

2.3. Functions $F_{\varphi f}$ and $F^{-1}_{\varphi f}$

Function $F_{\varphi f}$ describes the calculation of observable intensities f from phase differences φ of the interfering wave fields:[13]

$$F_{\varphi f}(\varphi, \boldsymbol{u}) = (f, \boldsymbol{u}) = (a(\boldsymbol{u}) + b(\boldsymbol{u}) \cos\varphi, \boldsymbol{u})$$

where $a(\boldsymbol{u})$ and $b(\boldsymbol{u})$ are the additive and multiplicative distortions (background intensity, speckle noise, varying fringe visibility).

A minimum of three intensities f_1, f_2, f_3 at an image point $\boldsymbol{u}$ with known phase shift of the reference beam are necessary for the calculation of phase differences with unknown distortions $a(\boldsymbol{u})$ and $b(\boldsymbol{u})$. In case of a constant phase shift of $\frac{\pi}{2}$ the function $\tilde{F}^{-1}_{\varphi f}$ for calculation of raw phases $\tilde{\boldsymbol{\varphi}}$ is:[15]

$$\tilde{F}^{-1}_{\varphi f}(f_1, f_2, f_3, \boldsymbol{u}) = (\tilde{\varphi}, \boldsymbol{u}) = \left(\tan^{-1}\frac{f_3 - f_2}{f_1 - f_2}, \boldsymbol{u}\right)$$

For calculation of the absolute phases φ the raw phases have to be unwrapped starting from a point with known absolute phase.[15] A continuous phase distribution is assumed.

2.4. Functions F_{af} and F^{-1}_{af}

Function F_{af} describes the calculation of intensity distributions given a parameter vector describing a flaw. It can be written as a composition of functions:

$$F_{af} = F_{\varphi f} \circ F_{d\varphi} \circ F_{ad}$$

In our system the inverse function F^{-1}_{af} cannot be calculated by combining the inverse problems introduced above as we do not have enough information for phase and displacement reconstruction. Instead, we use a feature based

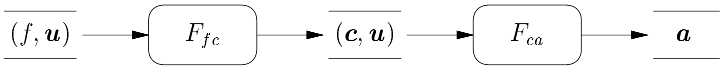

Figure 3. Data flow diagram of parameter estimation from interferograms using features

approach from the field of computer vision and pattern recognition.[16] From the observable intensities (pattern) we calculate features $\boldsymbol{c}$ which contain only information about the underlying phase distribution (function F_{fc}, see Fig. 3). The same kind of features are calculated from displacement vectors with function F_{ad}. In an iterative process (function F_{ca}), an estimation of a parameter vector is searched, which produces similar features to the features from measurement.

Function F_{af}^{-1} always must have a solution, as it is based on a well-defined physical process, but the solution is not unique. We have to add additional information to restrict the set of solutions. From a single interferogram the sign of the phase cannot be determined, but in most cases the sign is determined by the way the object is loaded. Displacements can be reconstructed uniquely if the displacement directions are known. In case of tank inspection we assume displacements being perpendicular to the surface. As already mentioned above, the uniqueness of function F_{ad}^{-1} is still a crucial point. In case of multiple solutions it is worth to investigate, if it is possible to obtain a unique solution by changing the type of load.

3. SYSTEM DESCRIPTION

In the last section we described the decomposition of the image formation and image analysis problem into several inverse and direct problems from a theoretical point of view. Now we focus on the realization of the analysis system. A top level data flow diagram of the system is shown in Fig. 4, a refinement of the parameter estimation process for the tank testing application is shown in Fig. 5. In the following, we give a brief description of the processes and show experimental results. For our experiments we use a replication of a typical satellite fuel tank with exactly known flaw parameters. The image processing algorithms are implemented on a standard PC (Pentium MMX 233 MHz), the finite-element simulation is executed on a SUN SPARC Ultra workstation.

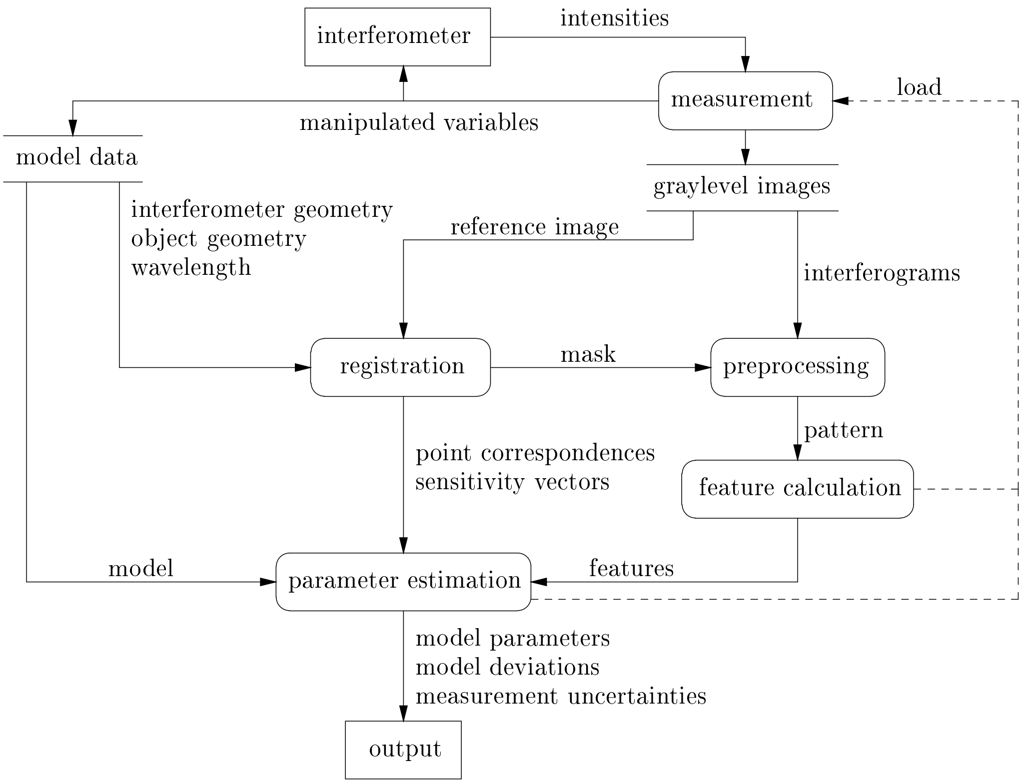

Figure 4. Top level data flow diagram of the system

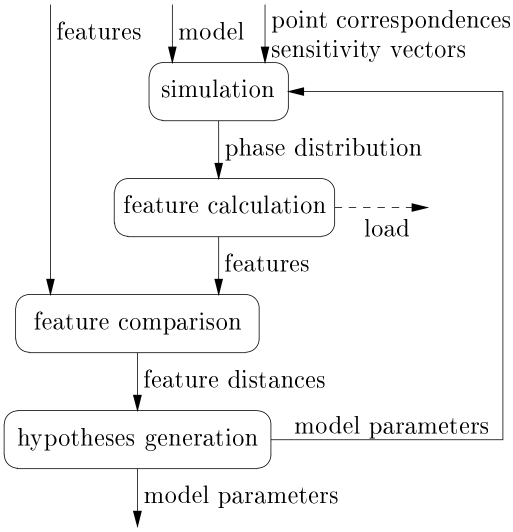

Figure 5. Data flow diagram of the parameter estimation process

3.1. Measurement

For the inspection of satellite fuel tanks a standard holographic setup is used (Fig. 6). To avoid repositioning problems and wet chemical processing we use photopolymers as holographic recording medium. Interferograms are digitized with a standard CCD camera and a standard PC frame grabber with PAL resolution. The tank is elastically deformed by changing internal pressure, the pressure is controlled by a PC. As no phase reconstruction is necessary, no phase shifting devices are needed. In Fig. 7 a holographic interferogram of the tank with flaw is shown.

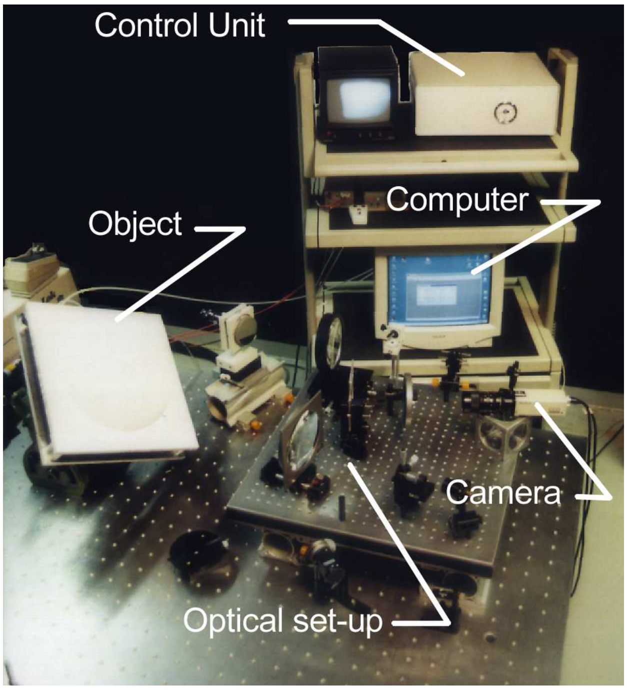

Figure 6. Experimental setup for HNDT of satellite fuel tanks

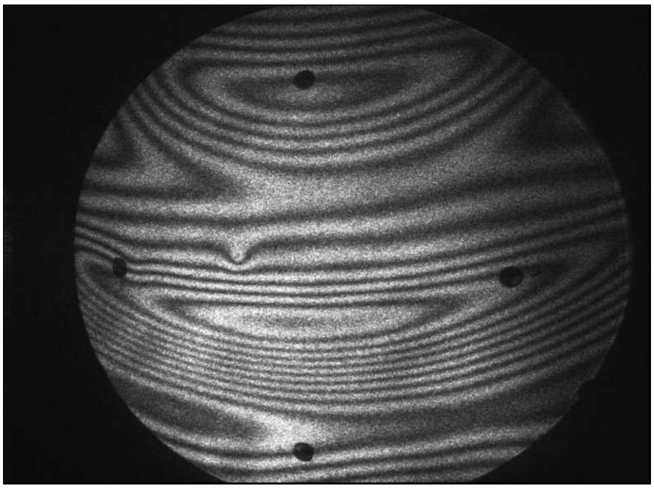

Figure 7. Holographic interferogram of a tank with flaw (eye-shaped pattern)

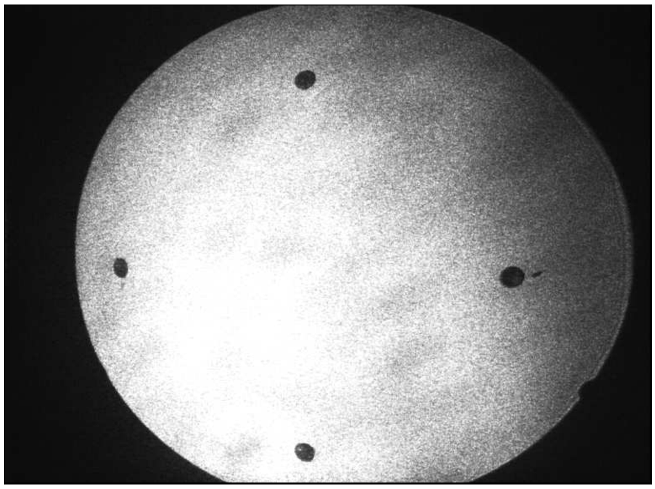

Figure 8. Reference image for registration

3.2. Registration

The problem of comparing two images of one scene recorded under different viewing conditions is usually called image registration in image processing.[16] For the comparison of features calculated from measurements and simulations it is necessary to find corresponding image and object points, i.e. a mapping of the tank surface to the image plane. If a pinhole camera model is assumed the mapping can be written as already described in section 2.2.

We use markers for the determination of the transformation matrix. The object pose is uniquely defined using six markers. If a rough estimation of the object pose is known, the solution can be constrained and four markers are sufficient. We use circular markers fixed on the tank surface which are made from light-adsorbing material. For the automatic extraction of the marker coordinates in the image, the tank is illuminated with the object wave only, so that no disturbing interferences complicate the detection. We apply image processing methods which are optimized for the segmentation of images with coherent illumination: Due to speckle noise it is not possible to apply a conventional edge detector. Instead, we first segment regions with low intensity and then search for neighbouring edges. Finally, marker centers are found by fitting ellipses to the edge image.

The object pose also is used for the calculation of sensitivity vectors, the propagation of the illumination beam is assumed to be known. Regions outside the quadrangle of the four markers are masked for the further calculation. In Fig. 8 the reference image for registration of a tank is shown. The complete registration process requires about 20 seconds.

3.3. Feature Calculation

In general, features should condense the essential information of a pattern concerning a given application. Here we are interested in the underlying phase of an interferogram, i.e. features should be independent of fringe contrast and background intensity. Furthermore, features should be independent of the absolute phase, as in most cases the absolute phase is not known or not very stable due to vibrations. We already proposed suitable features and methods for feature calculation from interferograms.[17] For each image point (x_o, y_o) we calculate a two-dimensional feature vector $\boldsymbol{c}(x_o, y_o)$ containing the features fringe density and fringe orientation.

Def.: fringe density and fringe orientation

given a quadratic region $B = \{(x,y) | x_1 \leq x \leq x_2 \wedge y_1 \leq y \leq y_2\}$ with $(x_o, y_o) \in B$ and following properties: $\forall\,(x,y) \in B$ holds: $\operatorname{grad}\varphi(x,y) = \boldsymbol{const} \neq \boldsymbol{0} \,\wedge\, a(x,y) = const \,\wedge\, b(x,y) = const \neq 0$
$\wedge\, \exists$ fringe ridge-line $\wedge\, \exists$ fringe ravine-line

$$\begin{aligned} \text{fringe density:} \quad \rho(x_o, y_o) &= \frac{\pi}{l} \quad \text{with } l = \text{distance between ridge-line and adjacent ravine-line} \\ \Rightarrow \quad \rho(x_o, y_o) &= |\operatorname{grad}\varphi(x,y)| \end{aligned}$$

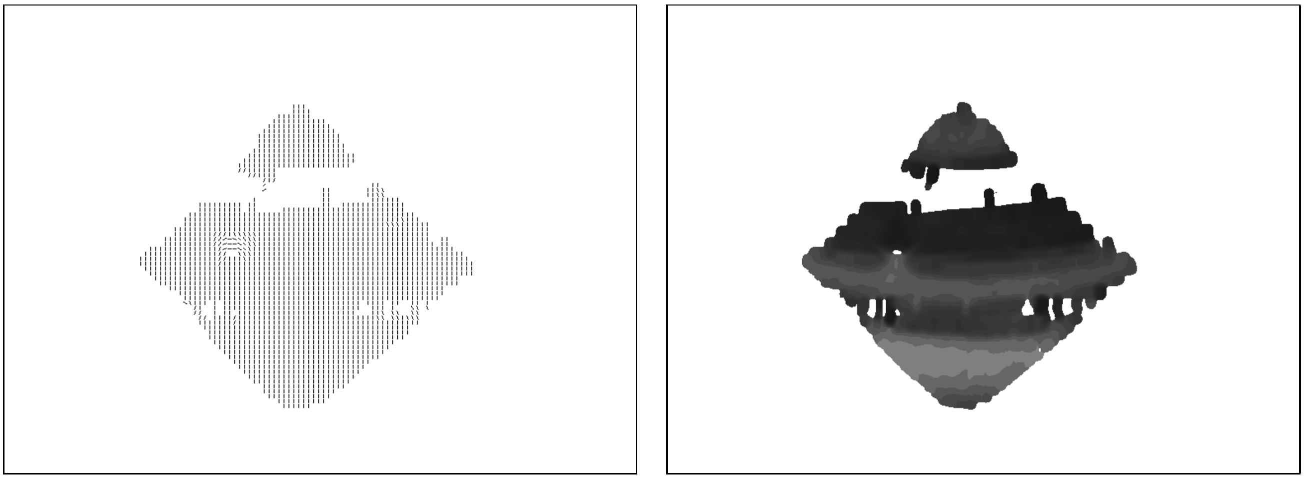

Figure 9. Features calculated from interferogram 7: fringe orientation (left), fringe density (right)

$$
\begin{aligned}
\text{fringe orientation:}\quad \alpha(x_o, y_o) &= \text{angle between y-axis and ridge-line} \\
\Rightarrow \quad \alpha(x_o, y_o) &= \begin{cases} \arctan \frac{\text{grad}_y \varphi(x_o, y_o)}{\text{grad}_x \varphi(x_o, y_o)} & : \ \text{grad}_x \neq 0 \\ \frac{\pi}{2} & : \ \text{grad}_x = 0 \wedge \text{grad}_y \neq 0 \end{cases} \\
\boldsymbol{c}(x_o, y_o) &= (\rho(x_o, y_o), \alpha(x_o, y_o))^t
\end{aligned}
$$

Briefly summarized from our previous work[17] features can be calculated robustly from interferograms as follows: First intensity ridge-lines and ravine-lines are segmented using only the directions of a gradient image of the interferogram. The gradient image is estimated from the interferogram using several window sizes depending on the homogeneneity of the gradient directions. Finally the distance between adjacent lines is estimated at each image point. Feature calculation from simulated phase distributions is less difficult, as it is possible to calculate the phase gradients directly and hardly any noise complicates the calculation.

In Fig. 9 an example for feature calculation from interferogram Fig. 7 is shown. The computation time is about 200 seconds. Regions where no features are available are either masked as they lay outside the marker area or they are masked due to unstable features, i.e. regions with inhomogeneous orientations or low fringe density. It can be shown that features from regions with low fringe density are quite sensitive to noise, furthermore the assumption of a constant phase gradient is easily violated. However a selective change of load allows to get a dense feature map (dashed line in Fig. 5).

3.4. Simulation

Since the described method assumes knowledge about the boundary conditions like used material, construction, applied load etc., it is possible to simulate the object deformation using the finite-element method (FEM). First, the geometry of the tank is meshed with the mesh generator of the finite-element program ANSYS 5.3, then the flaw is integrated automatically into the mesh, given a flaw parameter vector, and finally the deformation of the surface under internal pressure is calculated using the ANSYS FE-solver (Fig. 10).

During this procedure, the finite-element method delivers the deformation only for the edges of the element, i.e. the nodes. For the calculation of displacements at an arbitrary image point it is necessary to know the displacements at each corresponding object surface point, i.e. we have to interpolate between the nodes to get a continuous displacement distribution. Point correspondences are known from registration. The second problem we were faced with was that the entire strategy to solve the inverse problem is an iterative one, i.e. we have to calculate the deformation not only once, so it was unavoidable to reduce the simulation time from hours towards seconds. We achieved this by reducing the total area to be computed during the iteration to an smaller area of interest including the detected flaw indicating pattern only. In Fig. 11 a simulated interferogram of the tank is shown which is comparable to the measured one in Fig. 7.

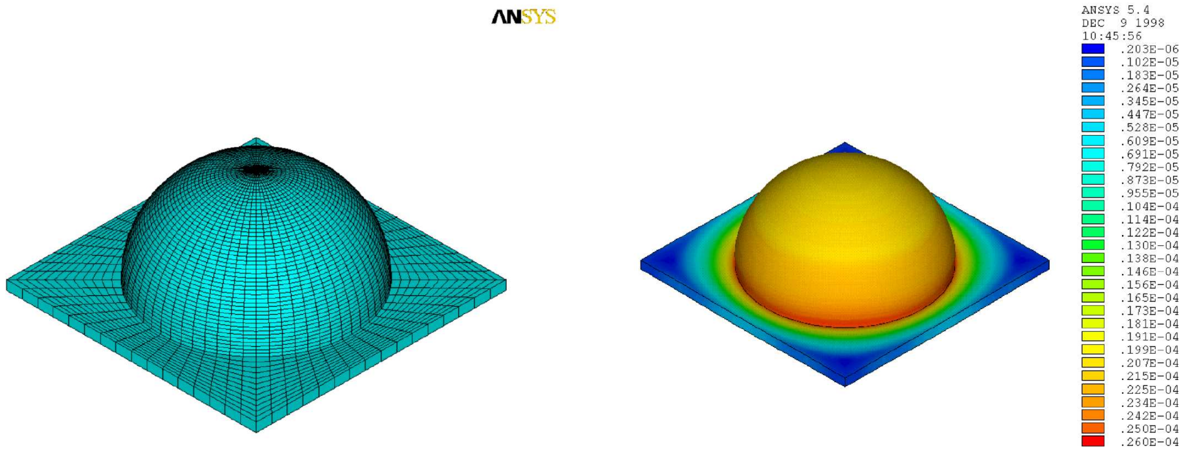

Figure 10. Finite-element-mesh of the tank and calculated deformation for internal pressure (magnitude of displacements in meters)

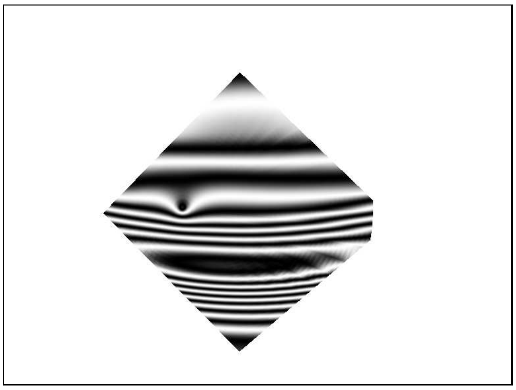

Figure 11. Simulation of interferogram with known flaw

3.5. Feature Comparison

The basic idea of solving the inverse problem F_{af}^{-1} is to compare features calculated from interferograms with features of simulated phase distributions and changing the parameter vector as long as the distance between the feature vectors is bigger than a given threshold. A crucial point is still the generation of suitable flaw hypotheses for an efficient iteration. This has to be done in future work. In principle the proposed method works if a complete parameter variation is done.

For feature comparison we are interested in a set S of image points (i, j) where the simulated deformations and the measured deformations do not coincide with a certain probability, given features and feature variances at (i, j):

$$
\begin{array}{rcl}
S & = & \{(i,j) | (\rho_{ij} - \tilde{\rho}_{ij})^2 > \sigma_\rho^2 \vee (\alpha_{ij} - \tilde{\alpha}_{ij})^2 > \sigma_\alpha^2\} \quad \text{with} \\
\alpha_{ij},\, \rho_{ij} & & \text{fringe orientation and fringe density from measurement} \\
\tilde{\alpha}_{ij},\, \tilde{\rho}_{ij} & & \text{fringe orientation and fringe density from simulation} \\
\sigma_\rho^2,\, \sigma_\alpha^2 & & \text{variances of features}
\end{array}
$$

If S contains no more image points, the parameter estimation process is terminated. Feature variances are estimated from interferograms of a calibration object with known deformation.

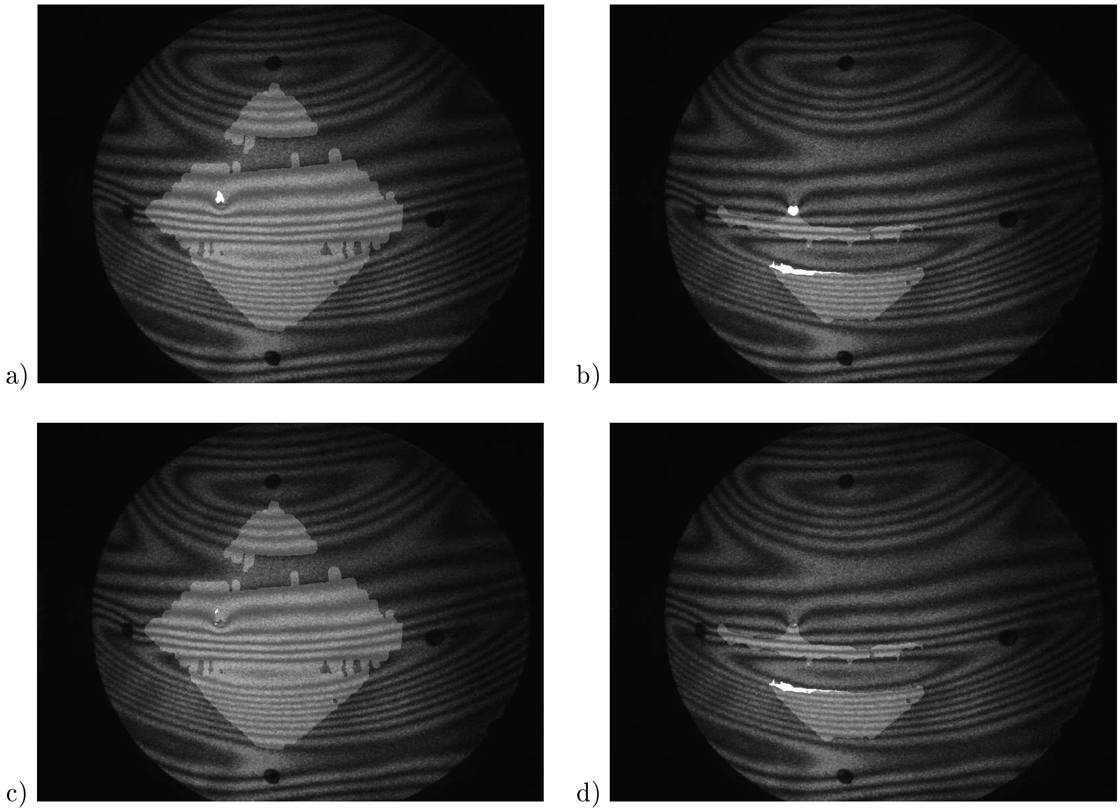

Figure 12. Comparison of features from measurement and simulation (gray overlays show evaluated regions, white overlays show regions with significant model deviations): a) fringe orientation, no flaw assumed, b) fringe density, no flaw assumed, c) fringe orientation, simulation with known flaw, d) fringe density, simulation with known flaw

In Fig. 12 some results for the tank example are shown. We compared features from interferogram Fig. 7 with a simulation of the tank without flaw and a simulation with flaw; the parameters of the flaw are exactly known. In the white regions the model deviates significantly from the measurement. It can be seen that in the flaw region there are significant deviations compared to the simulation without flaw. These deviations nearly vanish in case of a simulation with the correct parameter vector. However, there are some white regions which are falsely marked due to an incorrect simulation, i.e. the simulation still has to be improved. It takes about 80 seconds to calculate features from simulated phase distributions and to compare these features with features from measurement.

4. CONCLUSION

In this contribution we proposed a method for automatic HNDT of satellite fuel tanks. Here testing means to estimate parameters of a geometric flaw model from deformation behaviour of the tank surface, given a geometric model of the faultless tank. Deformation information is extracted from fringe patterns using image processing techniques. This kind of HNDT is an ill-posed inverse problem which is regularized using principles of active vision/metrology. In a feedback loop, features calculated from interferograms of different load states are compared with features from a finite-element simulation of the tank deformation with a hypothetical flaw. Different load states are useful for improvement of feature calculation and increasing sensitivity of fault detection.

Experiments have shown that the proposed method works in principle. The great advantage of the method is its flexibility, we do not need any sample to learn from. Further on we get a quantitative description of the flaw which makes it easy to decide if it is critical or not. Crucial point is a correct simulation of the tank which still has to be improved and the generation of suitable flaw hypotheses for a fast convergence which still has to be done in future works. Further on we have to investigate uniqueness of the solution and measurement uncertainties of the flaw parameters.

ACKNOWLEDGMENTS

This work is part of a joined project of Lehrstuhl für Mustererkennung and BIAS. It is financed by the Deutsche Forschungsgemeinschaft (DFG) under grants Pa 599 and Os 111 which is gratefully acknowledged.

REFERENCES

1. D. Marr, *Vision: A Computational Investigation into the Human Representation and Processing of Visual Information*, Freeman and Company, New York, 1982.
2. J. Keller, "Inverse problems," *American Mathematics Monthly* **83**, pp. 107–118, 1976.
3. M. Bertero and P. Boccacci, *Introduction to Inverse Problems in Imaging*, IOP Publishing Ltd., London, 1998.
4. B. Hofmann, "Ill-posedness and regularization of inverse problems," in *The Inverse Problem*, H. Lübbig, ed., pp. 45–66, Akademie Verlag, (Berlin), 1995.
5. W. Osten, W. Jüptner, and U. Mieth, "Knowledge assisted evaluation of fringe patterns for automatic fault detection," vol. 2004, pp. 256–268, SPIE, (Berlin), 1993.
6. T. Bischof, *Ein Beitrag zur Detektion und Bewertung von kugelförmigen Einschlüssen mit holografischer Interferometrie*, VDI Fortschrittsberichte, Reihe 8, Nr. 398, 1994.
7. W. Osten and W. Jüptner, "Digital processing of fringe patterns," in *Optical Measurement Techniques and Applications*, P. Rastogi, ed., pp. 51–85, Artech House, Inc., (Boston), 1997.
8. J. Hadamard, *Lectures on Cauchy's problem in partial differential equations*, Yale University Press, New Haven, 1923.
9. A. Tikhonov, "Solution of incorrectly formulated problems and the regularization method on cauchy's problem in partial differential equations," *Sov. Math. Dokl.* **4**, pp. 1035–1038, 1963.
10. A. Tikhonov and A. V.Y., *Solution of Ill-posed Problems*, (Transl. From Russian) Winston and Sons, Washington, 1977.
11. J. Aloimonos, I. Weiss, and A. Bandyopadhyay, "Active vision," *International Journal of Computer Vision* **2**(3), pp. 333–356, 1988.
12. E. Yourdon, *Modern Structured Analysis*, Prentice Hall, London, 1989.
13. T. Kreis, *Holographic Interferometry*, Akademie Verlag, Berlin, 1996.
14. O. Faugeras, *Three-Dimensional Computer Vision*, MIT Press, Cambridge, MA, 1993.
15. D. Robinson and G. Reid, *Interferogram Analysis*, IOP Publishing Ltd., London, 1993.
16. H. Niemann, *Pattern Analysis and Understanding*, Springer, Berlin, second ed., 1990.
17. T. Merz, D. Paulus, and H. Niemann, "Feature Extraction from Interferograms for Phase Distribution Analysis," in *Laser Interferometry IX: Techniques and Analysis*, M. Kujawinska, G. Brown, and M. Takeda, eds., vol. 3478, pp. 181–191, SPIE, 1998.